REPORT DOCUMENTATION PAGE

Form Approved
OMB No. 0704-0188

PLEASE DO NOT RETURN YOUR FORM TO THE ABOVE ADDRESS.

1. REPORT DATE *(DD-MM-YYYY)*	2. REPORT TYPE	3. DATES COVERED *(From - To)*
25-08-2005	REPRINT	

4. TITLE AND SUBTITLE
Comparison of Recent Measurements of Atmospheric Optical Turbulence

5a. CONTRACT NUMBER

5b. GRANT NUMBER

5c. PROGRAM ELEMENT NUMBER
62601F

6. AUTHOR(S)
George Jumper
Jean Vernin*
Max Azouit*
Herve Trinquet*

5d. PROJECT NUMBER
1010

5e. TASK NUMBER
0T

5f. WORK UNIT NUMBER
A1

7. PERFORMING ORGANIZATION NAME(S) AND ADDRESS(ES)
Air Force Research Laboratory/VSBYA
29 Randolph Road
Hanscom AFB, MA 01731-3010

8. PERFORMING ORGANIZATION REPORT NUMBER
AFRL-VS-HA-TR-2005-1124

9. SPONSORING/MONITORING AGENCY NAME(S) AND ADDRESS(ES)

10. SPONSOR/MONITOR'S ACRONYM(S)
AFRL/VSBYA

11. SPONSOR/MONITOR'S REPORT NUMBER(S)

12. DISTRIBUTION/AVAILABILITY STATEMENT
Approved for public release; distribution unlimited.

13. SUPPLEMENTARY NOTES
Reprinted from 36th Plasmadynamics and Lasers Conference, 6-9 June 2005, Toronto, Canada (AIAA 2005-4778)
*Department d'Astrophysique, Universite de Nice-Sophia Antipolis, Nice, France

14. ABSTRACT
A recent multi-sensor optical turbulence measurement campaign in the Haute-Provence region of France provided a unique comparison of optical turbulence sensors. Thermosondes from both the US and France were used, measuring temperature structure functions for 30 com, 95 cm, and 1 meter. In addition, turbulence was measured using a Generalized Scidar (GS) mounted on a 1.93 m diameter telescope at l'Observatoire de Haute-Provence (OH). The GS measures optical turbulence strength and altitude from the scintillation of binary stars observed over periods from several minutes to several hours. The GS has 300 m vertical resolution from 25 km down to nearly the opt of the telescope. This paper describes the instruments and compares their performance. While the instruments did not yield identical results, agreement was reasonable.

15. SUBJECT TERMS
Optical tuirbulence Thermosondes Generalized scidar

16. SECURITY CLASSIFICATION OF:			17. LIMITATION OF ABSTRACT	18. NUMBER OF PAGES	19a. NAME OF RESPONSIBLE PERSON
a. REPORT	b. ABSTRACT	c. THIS PAGE			George Y. Jumper
UNCL	UNCL	UNCL	UNL		19b. TELEPHONE NUMBER *(Include area code)* (781) 377-3148

36th Plasmadynamics and Lasers Conference
Toronto, Canada 6 – 9 June 2005
AIAA-2005-4778

Comparison of Recent Measurements of Atmospheric Optical Turbulence

George Y. Jumper*
Air Force Research Laboratory, Hanscom AFB, MA 01731-3010

And
Jean Vernin†, Max Azouit‡, and Hervé Trinquet§
Université de Nice–Sophia Antipolis, Nice, France

A recent multi-sensor optical turbulence measurement campaign in the Haute-Provence region of France provided a unique comparison of optical turbulence sensors. Thermosondes from both the US and France were used, measuring temperature structure functions for 30cm, 95cm and one meter. In addition, turbulence was measured using a Generalized Scidar (GS) mounted on a 1.93m diameter telescope at l'Observatoire de Haute-Provence (OH. The GS measures optical turbulence strength and altitude from the scintillation of binary stars observed over periods from several minutes to several hours. The GS has 300m vertical resolution from 25km down to nearly the top of the telescope. This paper describes the instruments and compares their performance. While the instruments did not yield identical results, agreement was reasonable.

Nomenclature

a	=	Constant	$\mathbf{r}$	=	Distance for structure function or C^{**} (m)
B_{bs}**	=	Difference in autocorrelation function	r_0	=	Fried's coherence length
b	=	Vertical stability of atmosphere (m^{-1})	S	=	Autocorrelation of detector impulse response
C	=	Autocorrelation function	S_{rr}	=	Power spectral density of turbulence
C_n^2	=	Index of refraction structure constant ($m^{-2/3}$)	v	=	Velocity
C_T^2	=	Temperature structure constant ($K^2m^{-2/3}$)	x	=	Distance in an arbitrary direction (m)
$D_y(\mathbf{r})$	=	Structure function of variable y	α	=	Constant
h	=	Altitude above ground (m)	χ	=	Constant for balloon motion (s^{-1}) See Eq. (15)
K	=	Turbulence wave number (m^{-1})	ΔH	=	Vertical Resolution
k	=	Wave number of light (m^{-1})	Δm	=	Difference in star magnitude
$\mathcal{L}$	=	Equivalent width of autocorrelation function	θ	=	Angular separation of binary star
N	=	Noise	θ_0	=	Isoplanatic angle
P	=	Pressure (Pa)	λ	=	Wavelength (m)
T	=	Absolute temperature (K)	σ_ν^2	=	Rytov varience

* Program Manager, Battlespace Environment Division, AFRL/VSBYA, Assoc. Fellow AIAA
† Faculty, UMR 6525, Departement d'Astrophysique, Parc Valrose 06034 Nice CEDEX 2, France
‡ Engineer, Departement d'Astrophysique, Parc Valrose 06034 Nice CEDEX 2, France
§ Research Faculty, Departement d'Astrophysique, Parc Valrose 06034 Nice CEDEX 2. France

I. Introduction

It is a well-known hypothesis that turbulence in the upper atmosphere is often the result of gravity (buoyancy) waves propagating into the upper atmosphere, growing in amplitude with altitude until they become unstable, then breaking into turbulence. Coulman *et al.*[1], made an early proposal of the wave – turbulence association in conjunction with the reporting of data from the thermosonde, a balloon-borne instrument that measures turbulence, which is described below. However, validation of the wave hypothesis has proven to be difficult. In July 2002, a study of the wave – turbulence interaction was performed by a French team, lead by Coulman's colleague, Jean Vernin, and a team from the Air Force Research Laboratory, Hanscom AFB, MA. This campaign utilized a number of sensors to detect gravity wave activity and optical turbulence. Gravity waves were sensed by the radiosonde instruments on the thermosondes[2]. Turbulence was sensed by the Generalized Scidar (GS) and the thermosondes. Reference 2 concentrates on the extraction of gravity wave information from the balloon data. This campaign provided a unique opportunity to compare the performance of the optical turbulence sensors, which is the focus of this paper.

A. Thermosondes

The thermosonde[3,4] has been used in optical turbulence research since 1971. It is attached to a meteorological radiosonde and is carried into the atmosphere by a balloon. The thermosondes flown by Air Force Research Laboratory personnel use two very fine resistance wire probes to measure the temperature difference across a 1m horizontal distance. Onboard electronics convert the temperature difference to a voltage signal, amplify and filter the signal, then perform a 4 to 8 second running average. The signal is then transmitted to the ground station along with the standard meteorological data: temperature, pressure, humidity, wind speed and direction sensed by the radiosonde[5,6].

The University of Nice team has flown thermosondes with a common origin to the US instruments, but which evolved separately through an early Italian design[7]. The French thermosondes use 4 wire sensors to measure two separate structure functions with lengths of 0.3m and 0.95m.

1. Thermosonde Theory

The use of the thermosonde to estimate atmospheric turbulence is based on the statistical theory of a randomly varying media. If two temperature sensors pass through the atmosphere a distance, r, apart along a path, x, the mean value of the square of the difference is defined as the temperature structure function, $D_T(r)$[8]:

$$D_T(r) = \left\langle \left[T(x) - T(x+r) \right]^2 \right\rangle \tag{1}$$

Structure functions of different lengths generally have different values. The theory that relates the different sizes comes from Kolmogorov. Kolmogorov hypothesized such a relationship for velocity fluctuations in a locally homogeneous and isotropic random field for scales less than the largest eddies known as the outer scale, L_0, which are on the scale of the turbulent kinetic energy source, and greater than the smallest eddies known as the inner scale, l_0, which are the scales of molecular energy dissipation. Kolmogorov reasoned that energy is transferred through inertial processes from the outer scale to the inner scale, the range between them is known as the inertial range. By dimensional arguments, Kolmogorov reasoned that, at equilibrium, longitudinal velocity fluctuations (along the direction of the vector r) in this range should satisfy the structure function relationship:

$$D_v(r) = C_v^2 r^{2/3} \tag{2}$$

where the constant C_v^2 is known as the velocity structure constant. While the condition of inertial range "equilibrium turbulence" defined above is not always present in the atmosphere, functional relationships with a power near 2/3 are surprisingly prevalent in the atmosphere. The 2/3 power in the structure function is equivalent to the one dimensional power spectrum (for positive frequencies) shown in Eq. (3). Since the power of the spatial wave number is -5/3, the Kolmogorov profile is either referred to as the -5/3 power law model or the 2/3 power law model.

$$S_{rr}(K) = 0.25 C_v^2 K^{-5/3} \tag{3}$$

Velocity turbulence in the presence of temperature gradients causes temperature fluctuations. Corrsin, Yaglom, and Obukhov[9] independently extended Kolmogorov theory to passive scalars, and showed that the structure function of conservative passive scalars should also follow the 2/3-power law. Therefore, the temperature structure function is expressed in terms of temperature structure constant, C_T^2.

$$D_T(r) = C_T^2 r^{2/3} \tag{4}$$

C_T^2 is not sufficient for prediction of turbulence disturbances to the propagation of electromagnetic radiation. These disturbances are based on the structure constant of the index of refraction of the air, C_n^2. Index of refraction is related to air density through the Gladstone Dale Constant. Turbulence in the free atmosphere is slow enough that variations in density are essentially due to the turbulent fluctuations of temperature, since pressure disturbances dissipate at the speed of sound. For microwave radiation, the variations in humidity must also be considered. Conversion of the temperature structure constant to the refractive index structure constant, C_n^2, depends on local pressure and mean temperature and the wavelength of the radiation that is being propagated. For radiation near the visible spectrum, and when the moisture contribution can safely be ignored (normal except right over a body of water) it is customary to use the formula[10*]:

$$C_n^2 = \left(a_d(\lambda) P / T^2\right)^2 C_T^2 \tag{5}$$

where $a_d(\lambda)$ = 79x10^{-8}K/Pa for visible and near-infrared wavelengths.

The theory described above implies a long run through a stationary, randomly varying temperature field in an equilibrium cascade. For the thermosonde, the conditions are varying as we ascend at anywhere from 3 to 8 m/s through what may or may not be stationary, homogeneous, equilibrium conditions. Therefore, we refer to our results as an estimate of the structure constants.

2. Thermosonde Hardware

There are differences in the way the U.S. and French apply Kolmogorov theory to the design of the thermosonde. The U.S. thermosondes have sensors 1 meter apart, as shown in Figure 1, measuring the one-meter structure function. The French thermosondes uses four probes to estimate the 0.3m and 0.95m structure functions, as shown in Figure 2. They sometimes use other lengths. Eq. 4 provides a relationship among the different sized structure functions, and used to compute the temperature structure constant, C_T^2, which should be independent of distance. The U.S. measurement across 1 meter simplifies the process since the structure constant is equal to the 1-m structure function. The French team uses the two structure functions to produce two estimates of the structure constant.

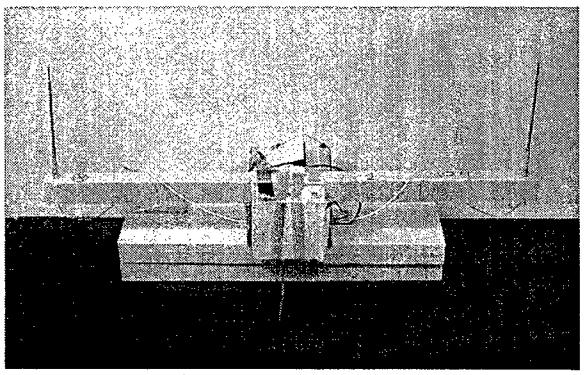

Figure 1. A U.S. thermosonde, with a 1-m distance between the two sensors on the boom. Radiosonde is taped in front, structure function electronics, batteries, and spare channel interface are behind.

Figure 2. The French thermosonde, with a 0.3m and a 0.95m distance between pairs of temperature sensors. Radiosonde electronics will be infront of container. other electronics behind.

* In this reference, one of the square symbols (^{2}) was inadvertently omitted. Please correct it!

A second design difference is the configuration of the resistance wires used to sense temperature. The resistance wire for the U.S. instrument is tungsten with a diameter is 3.45μm. The length of the U.S. wire sensor is less than 5mm, stretched between two conducting pins, as shown in Figure 3. The nominal resistance is 27Ω, and the temperature coefficient of resistivity of 0.00375 K^{-1}. The current through the wires is approximately 0.1A. The wires are approximately perpendicular to the airflow as the balloon lifts the instrument through the atmosphere; similar to typical "hot-wire" and "cold-wire" probes in wind tunnels. U.S. sondes are typically launched with a target ascent speed of 5 to 7m/s.

In the French design, the tungsten wire is 5μm diameter and 60mm long. It is threaded between 7 looped holders to form a conically shaped crown on the top of the vertical holder, as shown in Figure 4. The geometry of the design is intended to provide a sample of approximately a cubic centimeter of air. The nominal resistance is 220Ω at 20°C with a resistivity coefficient of 0.0035 K^{-1}. The current through each wire is 1mA. The target ascent speed is 4m/s.

In both designs a pair of sensor wires forms two legs of a Wheatstone bridge that generates a rapidly varying voltage based on the difference between the resistances of the wires. The signals are amplified, filtered, and then averaged. The U.S. design uses a circuit that performs a running average with a time-constant of about 4 to 8 seconds. The French design uses a circuit with a time constant for averaging of about a 1.25s^{1}. The French design has a duplicate circuit on the board for the second structure function.

Both teams currently use a Väisälä RS-80 Radiosonde with spare channel capability to send the running average of the structure function and some ancillary information down to the ground station with the typical atmospheric parameters sensed by weather balloon instruments: ambient temperature, pressure, relative humidity, and wind. Altitude is determined by the hydrostatic equation, corrected for humidity.

There is an interesting difference in design philosophy between the two thermosondes. In the case of the U.S. design, the field operators are laboratory employees, often engineers and technicians. Consequently, the field operations have been optimized for an expert staff in the field for final calibration and assembly of each package. In the case of the French design, the operators are often graduate students, and the packages have been engineered for ease of field operation. Consequently much of the calibration is performed back at the University of Nice laboratory. Probes are already paired to insure nearly identical resistance, color-coded and packaged for each thermosonde in groups of 4. In the field, the probes are fastened to the thermosonde with simple connectors to the color-coded receptors. The shielded electronics are slipped into a cardboard container which folds into an aerodynamic shape ready for flight.

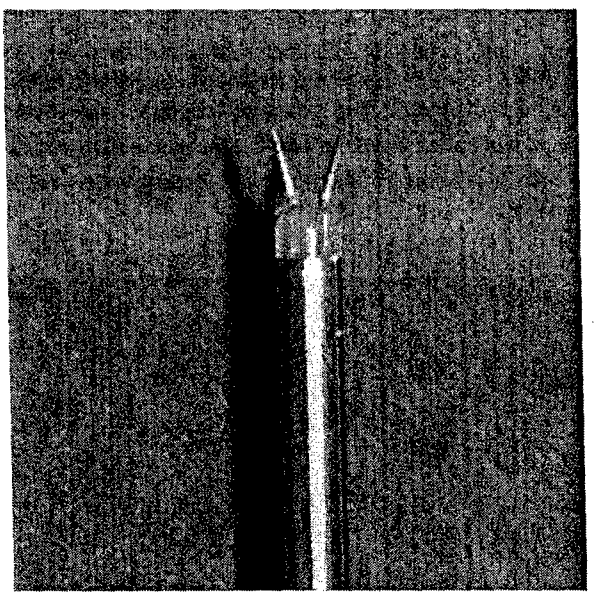

Figure 3. Sensor wire end of U.S. probe. Resistance wire is strung between the two electrodes.

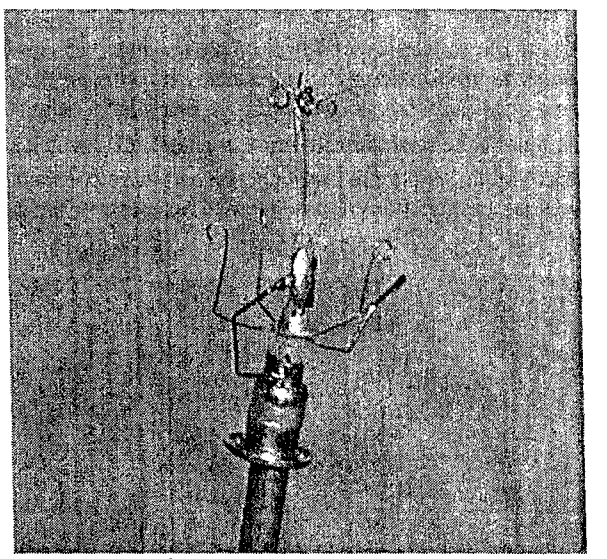

Figure 4. Sensor wire end of French probe. Resistance wire is strung from a top loop to a bottom loop and back to the top forming a conically shaped crown.

B. Generalized Scidar

A scidar is an optical method of measuring optical turbulence[11]. Short exposure time images such as shown in Figure 5 are analyzed to determine the profile of optical turbulence in the beam path. In the classical scidar, images from the telescope pupil are analyzed, which makes it insensitive to turbulence close to the ground because the scintillation variance is proportional to $h^{5/6}$, where h is the altitude above the ground of the turbulent layer (acting as a phase screen)[12]. In the GS the plane of the detector is made the conjugate to a plane (analysis plane) at a distance h_{gs}, on the order of a few kilometers, below the telescope pupil $\left(h_{gs} > 0\right)$. With a GS, the turbulence at ground level (including the telescope dome) becomes detectable because the distance relevant for scintillation produced by a turbulent layer at an altitude h is now $\left|h - h_{gs}\right|$ above the analysis plane.

The autocorrelation of the scintillation produced by a turbulent layer consists of three components: one is centered at the origin, and the two others are separated by $\vec{\theta}H$ and $-\vec{\theta}H$, respectively, where $\vec{\theta}$ is the angular separation of the double star, and $H = \left|h - h_{gs}\right|$, which is equal to $h - h_{gs}$ for the case of interest, since $h_{gs} < 0$. As the different turbulent layers are statistically independent, the contribution of each one is added, and the total theoretical autocorrelation function can be written as:

$$C^{**}(\mathrm{r}) = \int_0^\infty dh C_n^2(h)\left\{aC(\mathrm{r},h) + b\left[C\left(\mathrm{r} - \vec{\theta}h, h\right) + C\left(\mathrm{r} + \vec{\theta}h, h\right)\right]\right\} \tag{6}$$

where $C(\mathrm{r},h)$ represents the autocorrelation of the scintillation of a single star produced by a layer of unit C_n^2, at an altitude h. The factors a and b are given by

$$a = \frac{1+\alpha^2}{(1+\alpha)^2}, \quad b = \frac{\alpha}{(1+\alpha)^2}, \quad \alpha = 10^{-0.4\Delta m} \tag{7}$$

where Δm is the magnitude difference of the double star.

Eq. (6) shows that all the information needed to retrieve $C_n^2(h)$ is contained in a radial section of $C^{**}(\mathrm{r})$ along the double star separation. Furthermore, we wish to eliminate the central peak where the contribution of each layer is undistinguishable from that of the others, as they are added, and it contains the uncorrelated noise. For this reason, the difference of the sections of the measured autocorrelation function parallel and perpendicular to the stars separation, $C_{\parallel}^{**}$ and $C_{\perp}^{**}$ respectively, are calculated. This difference can be written[13]:

$$\begin{aligned} B_{bs^{**}}(x) &\equiv C_{\parallel}^{**} - C_{\perp}^{**} \\ &= \int dh K(x,h) C_n^2\left(h - h_{gs}\right) + N(x) \end{aligned} \tag{8}$$

where $N(x)$ is the noise, and the kernel $K(x,h)$ is a radial section of $C\left(\mathrm{r} - \vec{\theta}H, H\right) * S(\mathrm{r})$ along the direction $\mathrm{r} \| \theta$, where $S(\mathrm{r})$ is the autocorrelation of the impulse response of the detector. By measuring $B_{gs^{**}}(x)$, calculating theoretically $K(x,h)$ and knowing h_{gs} as well as an estimate of the noise variance, Eq. (8) (of Fredholm type) is inverted to retrieve $C_N^2(h)$ using a maximum entropy algorithm. The inversion is simplified by the diagonal elements in $K(x,h)$ along the line $x = \theta\left(h - h_{gs}\right)$.

Important features of the GS should be noted: The space between the telescope pupil and the analysis plane is turbulence-free because it is virtual. The $C_n^2(h)$ measurements are independent of static optical aberrations, as they are cancelled out in the data analysis. The vertical resolution of the retrieved $C_n^2(h)$ profiles is given by[14]

$$\Delta H = \frac{\mathcal{L}\left(|h-h_{gs}|\right)}{\theta} = \frac{0.5}{\theta}\sqrt{\lambda|h-h_{gs}|} \tag{9}$$

where $\mathcal{L}\left(|h-h_{gs}|\right)$ is the equivalent width of the scintillation spatial autocorrelation function, related to the first Fresnel zone, and λ is the wavelength. As an example, the resolution achieved at ground level $(h=0)$ when observing the double star 95 Herculis (θ = 6.2 arcsec), with the analysis plane at $(h_{gs}=-4km)$, is ΔH = 740m. But the maximum entropy method increases the vertical resolution by a factor of about 2, which leads to a final vertical resolution of about 300m.

A typical $C_n^2(h,t)$ plot, shown in Fig. 6, is obtained using binary star γ Del with angular separation of θ = 9.3 arcsec. Many layers are detected at 1km, just above ground level, at 4km, and then 4 layers are visible between 10 and 15km. The vertical resolution is, as expected, about 300m. The temporal resolution is about 21s.

The GS performance depends on the size of the telescope mirror. The separation distance of the two star images is equal to the angular separation of the stars times the altitude of the turbulence layer. The factors that limit the maximum angular separation are: the images migrate on the image based on the wind velocity of the turbulent layer, so the distance between the outer images must be limited to a fraction, *f*, of the mirror diameter; and it is desired to measure turbulence layers up to 25km. The maximum separation is $\theta_{max} = f\,D/h_{max}$ where D is the mirror diameter. The new very large telescopes permit the use of much greater star separations, opening up the opportunity for star pairs that are not necessarily binary stars, permitting longer coverage times at higher zenith angles.

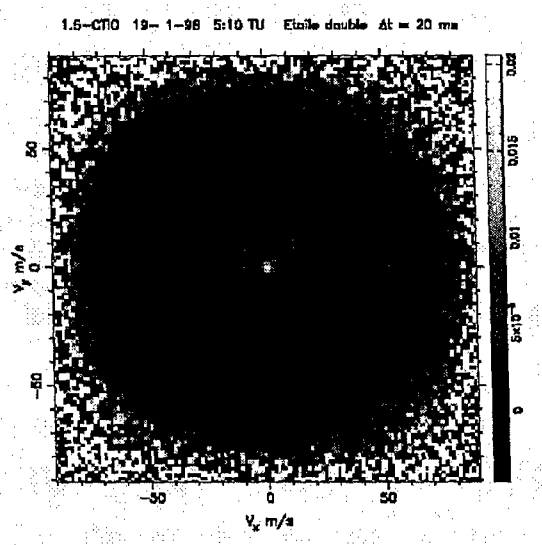

Figure 5. Cross-correlation of scintillation images separated by 20ms, obtained with the double star κPupis, of angular separation of 9.9 acrsec. The coordinates of the central peak of each of the 3 triplets give the wind velocity of the corresponding layer.

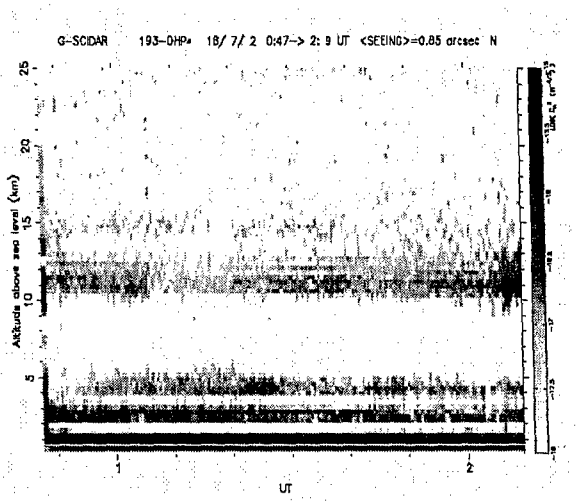

Figure 6. Graphical display of GS results showing a time series of optical turbulence profiles up to 25km above OHP as a function of time for a period from before 1:00 to after 2:00UTC on 18 July 2002. The color scale depicts C_n^2 levels from ~$1x10^{-18}$ (white) to $1x10^{-16}$ $m^{-2/3}$ (dark blue).

II. The Experiments

The campaign started the evening of 17 July 2002, and lasted until the morning of 24 July 2002. Data were taken from two separate locations. GS optical data and thermosonde data were acquired at l'Observatoire Haute Provence (OHP) (latitude 43.9N and longitude 5.71E and altitude 630m MSL). Thermosonde data were also acquired at the private SIRENE Observatory located at Lagarde d'Apt (designated in this paper as "APT") (latitude 44.0N and longitude 5.5E and altitude 1,100m MSL).

The Generalized Scidar (GS) was mounted on the 1.93m diameter telescope at OHP. The GS provides continuous nighttime profiles of turbulence at 300m-resolution from telescope altitude up to 25km. Thermosondes were launched at the OHP site and at the APT site, which is 20km W by NW of OHP. Gravity wave activity was deduced from temperature, horizontal wind velocity and balloon ascent rate measured by radiosondes, which are part of the thermosonde system. Over the course of the week, the US team launched 8 sondes from APT, the French team launched 23 thermosondes from APT and 19 from OHP, and acquired 4317 GS files of approximately 20s duration each.

On the night of 19-20 July, two flights were made with a U.S. and French thermosonde attached to the same balloon. In one, the thermosondes were secured next to each other with the booms at equal altitude 50m below the balloon. In the second flight the French thermosonde was located 50m below the balloon and the U.S. thermosonde was located 50m below the French instrument.

III. Analysis and Results

A. Thermosondes

1. US and French Thermosonde Comparison

The first dual thermosonde flight, with the US and French instruments right next to each other 50m below the balloon, provided some very worthwhile data for comparison;. The second flight with the US instrument 50m below the French instrument did not work as well. There appeared to be interference affecting the French instrument, especially at the higher altitudes. Therefore, only the first flight will be used for comparison. Because of the differences in the signal averaging time between the US and the French instruments, the actual time series of profile of data appear quite different. Therefore, for purposes of comparison, each C_n^2 profile has been averaged over 300m bins. The results for the C_n^2 from the two French structure functions (30cm and 95cm) and the single 1m structure constant from the US instrument are shown in Figure 7. With a few regions of disagreements, the comparison is quite encouraging. The agreement between the US (1m) and the FR 95cm is very close, which might be expected since these probes were very close together. The C_n^2 from the 30cm data is also close to the other data, except for the region between 8 and 12km, where these data exceed the results from the larger structure functions by quite a bit. This could be the result of some very non-Kolmogorov behavior, say a region of very low turbulence that still has a large amount of very small-scale turbulence. However, it is not a good idea to put too much credence on the results from a single flight. It is possible that the electronics for that structure function experienced a high noise condition for that altitude range. There are a few places where the US instrument is showing some regions of higher turbulence that the FR instrument does not agree: for instance near 18km and near 20km.

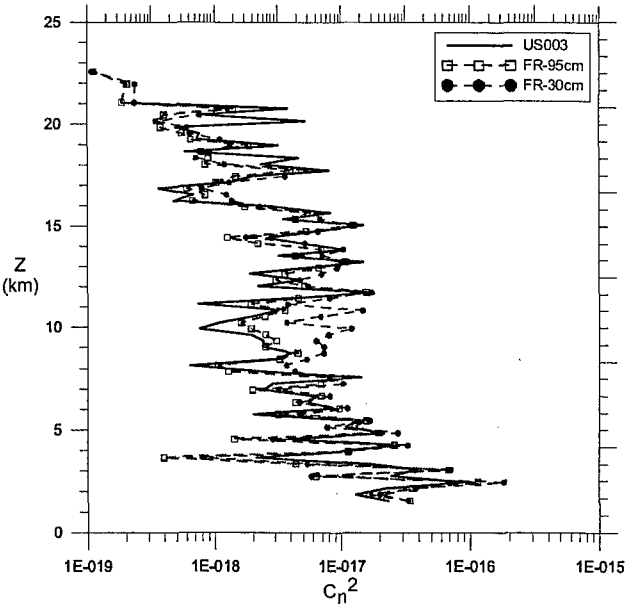

Figure 7. Comparison of C_n^2 computed from French 95cm, 30cm, and US 1m structure functions. Data have been averaged over 300m bins. Balloons launched from Apt on 19 July 2002.

The impact of turbulence on light passing through the atmosphere is a function of integrals through the region. Some optical performance integrals are: The Rytov variance, σ_χ^2 a measure of the amount of scintillation of the light; Fried's Coherence length, r_0 an indication of the largest uncorrected telescope lens that can be used effectively; the isoplanatic angle, θ_0, a

measure of the maximum angle of that one could expect coherence between an incoming beam from a source and an outgoing beam. The latter would apply to the ability to use adaptive optics to correct observed phase distortions. For light coming down through the atmosphere from a source at great distance, say a star, the equations for these three performance parameters are:

$$\sigma_\chi^2 = 0.56k^{7/6}\int_0^L C_n^2(\eta)(L-\eta)^{5/6}\,d\eta \tag{10}$$

$$r_0 = \left[0.423\,k^2\int_0^L C_n^2(\eta)\,d\eta\right]^{-3/5} \tag{11}$$

$$\theta_0 = \left[2.91\,k^2\int_0^L C_n^2(\eta)\eta^{5/3}\,d\eta\right]^{-3/5} \tag{12}$$

where k is the wave number of the light ($k = 2\pi/\lambda$), η is the length along the beam path, and L is the total beam path. Each integral is terminated at an altitude where the C_n^2 is so small that it no longer contributes to the integral.

The three performance parameters were evaluated for the three C_n^2 profiles. There were some rather large differences in the three C_n^2 results near the ground, where turbulence is very high, but high reading can come from instrument, so the performance integrals were evaluated from 2km up to 21km – the maximum altitude of data from the US instrument. The results are shown in Table 1. The agreement between the US and the French instruments are reasonably close, as expected from the C_n^2 profiles. The FR 30cm result is worse for some quantities, but not bad in others. Since each performance parameter has different weighting with distance, the results respond accordingly. Whereas r_0 is equally weighted with altitude, the weighting for θ_0 decreases with altitude, and the weighting for σ_χ^2 increases with altitude until the integration stops due to insignificant C_n^2.

Table 1. Comparison of optical performance parameters from the three sources of C_n^2, the US 1m structure function, and the French 30cm and 95cm structure functions.

C_n^2 Source	r_0 (cm)	θ_0 (μ rad)	σ_χ^2 (n.d.)
US 1m	25.31	11.58	0.019
FR 30cm	20.80	10.95	0.023
FR 95cm	25.00	13.59	0.016

2. Kolmogorov Hypothesis

As mentioned above, the French use the Kolmogorov hypothesis to compute two estimates of C_T^2 from the two structure functions, $D_T(.3)$ and $D_T(.95)$, using Eq. (4). Many groups have studied the applicability of Kolomogorov's hypothesis for turbulence in the atmosphere. Two groups have compared many structure functions obtained from ascending[15] or descending[16],[17] balloons. The French thermosondes provides another opportunity to test the applicability of the hypotheses to atmospheric temperature turbulence. A cross-plot of C_n^2 from $D_T(.3)$, designated as C_n^2–30, to C_n^2 from $D_T(.95)$ C_n^2–95 for each time is shown in Figure 8. The straight line is the identity line. A first impression is that the points generally follow the Kolmogorov trend, with a spread in the data of about an order of magnitude about identity. It also appears that the

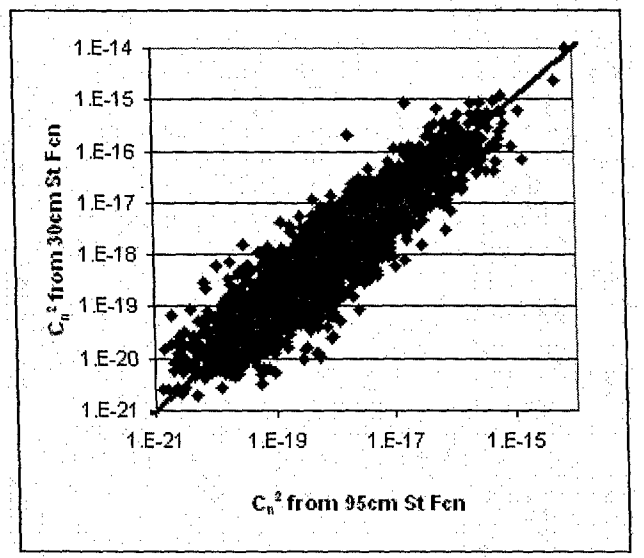

Figure 8. Cross-plot of C_n^2 from the 30cm structure function to C_n^2 from 95cm structure function from each data time line.

lowest values of C_n^2 might have higher values from the 30cm function. These C_n^2 values could be analyzed further; however, this could be misleading. Recalling the strong atmospheric weighting when converting from C_T^2 to C_n^2 from Eq. (5), it is clear that the altitude plays a very strong roll in the lowering C_n^2 as altitude increases. Therefore, there is strong altitude dependence in the placement on the abscissa of the plot.

An alternate approach is to compare temperature structure constants, C_T^2 from each probe pair. The result is shown in Figure 8. Again, there is an impression of general agreement with the identity line, and, perhaps, an even stronger impression that at low values of C_T^2, the values for C_T^2–30 are larger than the corresponding values from the C_T^2–95. Next, the ratio of the two values of C_T^2 for each time step (C_T^2–30 / C_T^2–95) is compared to C_T^2–95 in Figure 9. Here, it is quite obvious that C_T^2–30 exceed C_T^2–95 at lower magnitudes, but that the ratio decreases as the C_T^2 values increase, crossing unity near the middle of the population, but continue to decrease as C_T^2 increases.

Exploring this further, the data were separated into bins of half an order of magnitude. Next the average value of the ratio was computed for each bin, and the percent of the total population of 3870 pairs of C_n^2 values was computed for each bin. These results are shown in Table 2 and Figure 10. This appears to be an almost log normal population centered in the bin: $1x10^{-5} < C_n^2 < 1x10^{-4.5} = 3.6x10^{-5}$. It is clear that the average ratio is quite high at the smallest values of C_n^2 but descends to near unity by 10-4 to 10-3.5, remains near there as C_n^2 increases, until the final bin, where it reduces to 0.58. There are only 5 points in this bin, so it is hardly a statistical sample, and is probably not significant. One interpretation of these results is that for the lowest levels of turbulence, the larger scales have significantly diminished while there remains measurable activity in the very small scales. At this point, this is mere speculation.

Table 2. The ratio of C_T^2 based on the 30cm structure function to that of the 95cm structure function for bins of half an order of magnitude each from $10^{-6.5}$ to 10^{-2}. Also shown is the percent of total population in each bin.

Bin Min ($\log_{10}$)	Bin Max ($\log_{10}$)	Avg. Ratio .3m to .95m	Population (%)
- 6.5	- 6	4.71	2.2
- 6	- 5.5	3.22	10.9
- 5.5	- 5	2.31	21.3
- 5	- 4.5	1.8	27.6
- 4.5	- 4	1.46	20.6
- 4	- 3.5	1.18	11.7
- 3.5	- 3	0.903	4.4
- 3	- 2.5	0.899	1.08
- 2.5	- 2	0.58	0.13

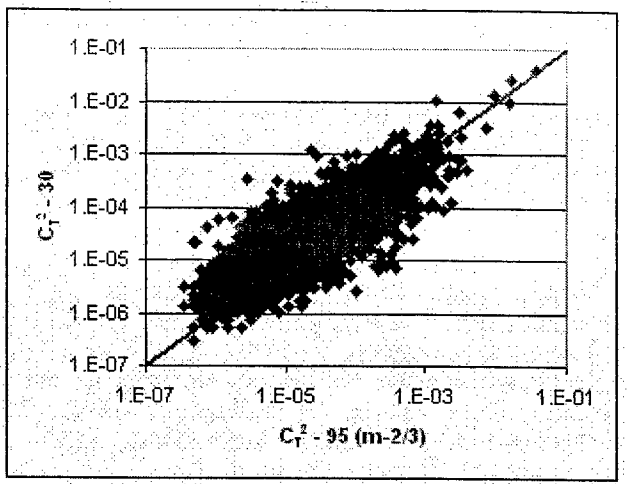

Figure 8. Comparison of C_T^2 from the 30cm structure function to C_T^2 from 95cm structure function from each data time line.

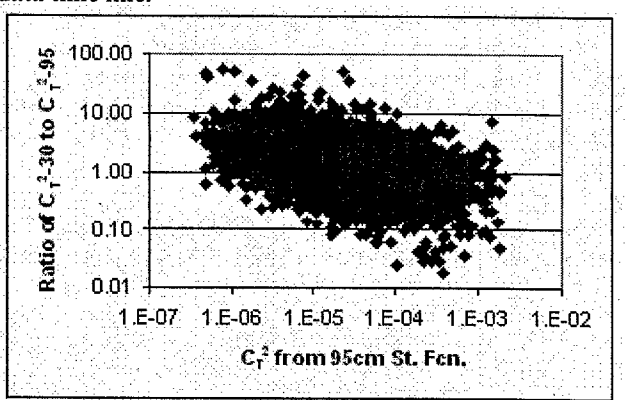

Figure 9. Comparison of the ratio of C_T^2 from the 30cm structure function to C_T^2 from 95cm structure function from each data time line vs. C_T^2 from the larger function.

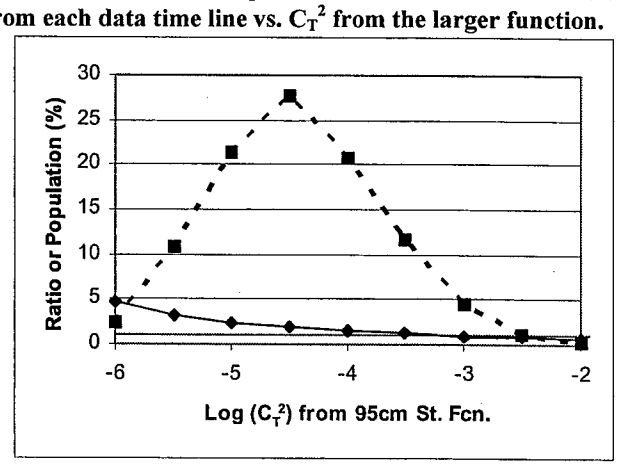

Figure 10. Average of ratio of C_T^2 from the smaller structure function to the larger vs. $\log_{10}$ of C_T^2 binned by half magnitudes (diamonds). Unity is shown as the solid line near the bottom. Also shown is the population distribution in the bins as percent.

By analyzing C_T^2 instead of C_n^2, does not imply that the range of C_T^2 is independent of altitude. A plot of all the C_T^2 values from the flight we have been analyzing, designated VOL267, is shown in Figure 11. The values from the larger structure function are shown in dark diamonds, and those from the smaller are shown in light circles. The minimum C_T^2 values recorded are typically the noise floor of the instrument that does not directly depend on altitude, but the electronic components of the instrument, which may be dependent on altitude related quantities such as the temperature of the electronics compartment. In Figure 11, it appears that the noise floor of the larger structure function is lower than for the smaller structure function. The maximum values of C_T^2 are generally a function of the slope of the potential temperature profile and the strength of the turbulence. The higher values at low altitudes are indicative of the high turbulence levels near the surface, and the generally higher values in the stratosphere relate to the increase in the gradient of the potential temperature.

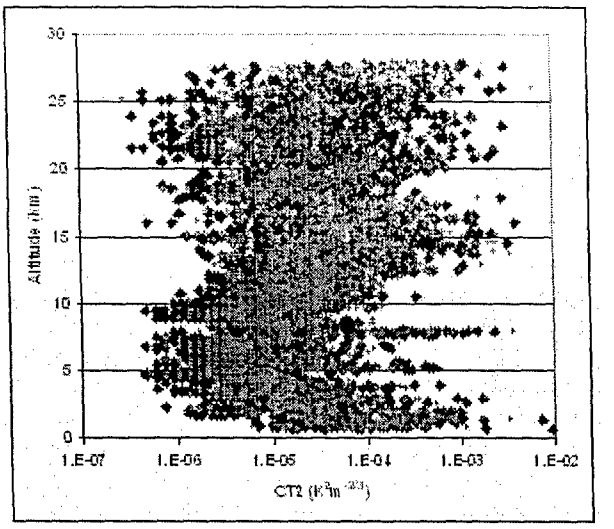

Figure 11. Profiles of C_T^2 from the smaller structure function (small lighter circles) and from the larger (darker diamonds) for flight VOL267.

These results are from one balloon ascent only, and are not meant to imply a complete analysis. Rather this has been presented to give the reader an appreciation for the wealth of information available from the collection of more than 500 flights of the French thermosondes.

B. Scidar and Thermosondes

A comparison of a time series of optical turbulence for the GS is shown next to a C_n^2 profile from a thermosonde launched early in the period shown in the GS plot. The output is in fair visual agreement, particularly in the lower

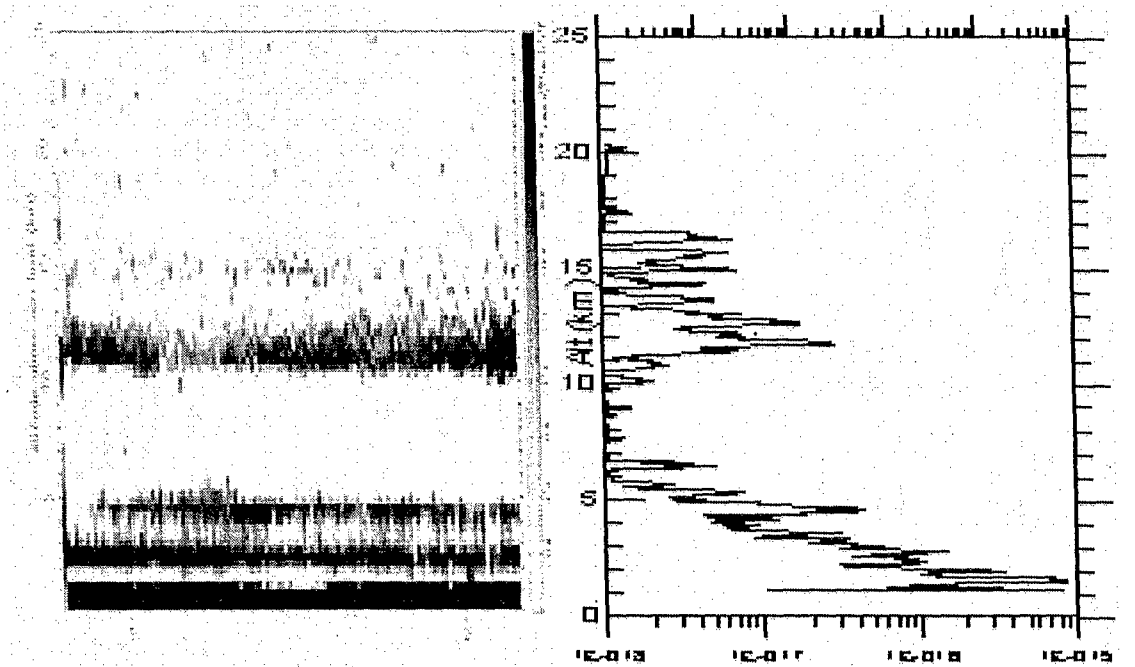

Figure 12. A comparison of C_n^2 as measured by the GS (left) and from a thermosonde (smoothed with a 300m window). The GS data is a time series over a period of an hour and 20 minutes on the evening of 18 July 2002. The thermosonde was launched during the period of the GS data.

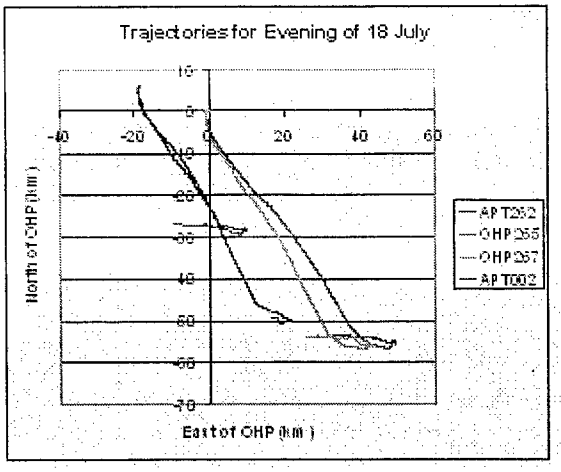

Figure 13. The trajectories of 5 thermosondes launched on the evening of 18 July.

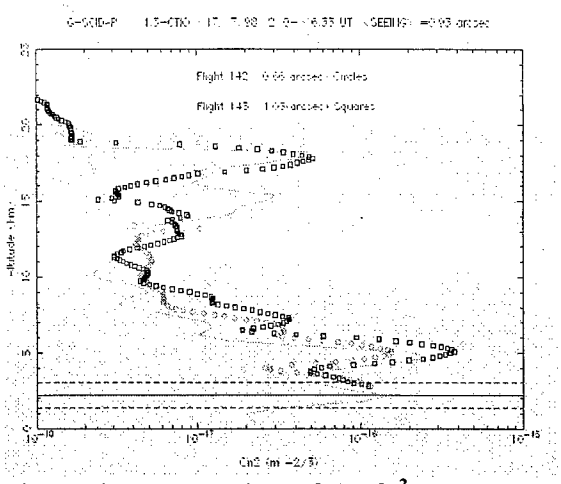

Figure 13. A comparison of the C_n^2 measured by the GS (solid line) located at the altitude of the lower dashed line and 2 thermosondes launched from the upper dashed line[14]. One thermosonde is shown by circles, the other by squares.

atmosphere. Both plots show high values near the surface, a higher band from 2 to 3km, a band between 4 and 5km, and the heavy band near the tropopause between troposphere and stratosphere know for high levels of turbulence.

Above the tropopause, the comparison breaks down. This is at least in part due to the fact that the thermosondes are drifting away from their launch sites with the horizontal velocity of the prevailing wind. The trajectories of 5 balloons launched that night are shown in Figure 13. The telescope is located at the origin of the plot. Since the GS is usually observing double stars at a zenith angle of less than 45°, the outer bounds of the GS data would be a circle of 25km radius drawn around the origin.

A quantitative comparison of the measurements of the GS to those of the thermosonde is shown in Figure 14 from reference 14. The figure compares the GS located at the lower of the two dashed lines to two balloons from a campaign in Chile in 1998. The comparison is generally good, with some discrepancies at the higher altitudes, probably due to the drift of the balloon described above.

IV. Conclusion

The 2002 Campaign in the Haute-Provence region of France provided an excellent opportunity to compare turbulence results from three methods of measuring atmospheric optical turbulence: the generalized scidar (GS), and two versions of the thermosonde, the design used by the French team and that used by the US team. In one flight, the two different thermosondes were lashed together and flew 50m beneath the ascending balloon. The results of C_n^2 as determined by the 1m structure function of the US instrument closely matched the C_n^2 data from the 0.95m structure function of the French instrument. The data from the 0.3m structure function of the French instrument generally agreed quite well also, except for a portion of the atmosphere where it showed considerably higher turbulence than the other two readings for an unknown reason. Optical performance parameters from the three structure functions generally agreed quite well, especially Fried's coherence length for the 0.95m and 1m structure functions which only differed by 1.25%.

The presence of two structure functions on the French instrument provides an opportunity to test Kolomogorov's hypothesis of the relationship among structure functions of different sizes. Only data from one thermosonde was analyzed. The analysis showed fair agreement with the hypothesis, but showed increasing divergence at the lower values of structure function, with the smaller structure function yielding higher than the values predicted by the hypothesis. This result from a single ascent demonstrates the wealth of data that is routinely available from the French design to more fully explore the applicability of the Kolmogorov hypothesis to various atmospheric conditions.

The agreement of the GS with the balloons is especially good at the lower altitudes. At higher altitudes the agreement is not as good, but the thermosondes typically drift out of the region of GS viewing and are probably experiencing different atmospheric conditions. The GS is a remarkable instrument which provides nearly continuous profiling of the turbulence in the atmosphere, except when blocked by cloud cover or when binary stars are not in the viewing region. Measurement by GS is clearly the instrument of choice, at least whenever a telescope of sufficient diameter is available.

V. Acknowledgement

The authors would like to acknowledge our hosts for these experiments, the staff at L'Observatoire de Haute-Provence (OHP) and F. Bardin and the other members of the staff at the Sirene L'Observatoire, Lagarde d'Apt. France.

The Air Force Research Laboratory portion of the Campaign was funded by the Air Force Office of Scientific Research, Laboratory Task 97PL007. The French team was funded by the International Research Initiative funds of the AFOSR.

Finally, we thank Dr. Beland, our branch chief and his staff for all their technical advise and support, Mr. Paul Tracy, Chief Engineer. We are indebted to the members of the field team, Aziz Ziad, Karim, Benkhaldoun Zouhair, AFRL manager, Anthony Ratkowski, AFRL electrical engineer Michael Curry, AFRL technician, John Glass,

References

[1] Coulman C.E., J. Vernin, and A. Fuchs, "*Optical seeing – mechanism of formation of thin turbulent laminae in the atmosphere*", Applied Optics, Vol. 34, No. 24, pp. 5461-5474, 1995.

[2] Jumper, G.Y, E.A. Murphy, A.J. Ratkowski, and J. Vernin, "Multi-sensor Campaign to Correlate Atmospheric Optical Turbulence to Gravity Waves," AIAA-2004-1077, *42nd AIAA Aerospace Sciences Meeting & Exhibit*, Reno, NV, 5–8 Jan 2004.

[3] Titterton, P.J., Mallery, L.E., and Arken, T.A., *Lightweight Thermosonde System*, GTE Sylvania, Inc., Final Report, (Contract NAS5-11493) December 1971.

[4] Bufton, J. L., *A radiosonde thermal sensor technique for measurement of atmospheric turbulence*, Goddard Space Flight Center, NASA TN D-7867, February 1975.

[5] Brown, J.H., R. E. Good, P.M. Bench, and G. Faucher, "Sonde measurements for comparative measurements of optical turbulence," Air Force Geophysics Laboratory, AFGL-TR-82-0079, ADA118740, NTIS, 1982.

[6] Jumper, G.Y., H.M. Polchlopek, R.R. Beland, E.A. Murphy, P. Tracy, K. Robinson, "Balloon-borne measurements of atmospheric temperature fluctuations", AIAA-97-2353, 28th Plasmadynamics and Lasers Conference, June 23-25, 1997, Atlanta, GA

[7] Barletti R., G. Ceppatelli, L. Paternò, A. Righini, and N. Speroni, "Astronomical site testing with balloon-borne radiosondes," Astron. Astrophysics. Vol. 54, 649-659, 1977.

[8] Beland, R., "Propagation through Atmospheric Optical Turbulence", *The Infrared & Electro-Optical Systems Handbook*, J. Acetta and D. Shumaker, ex. eds., *Vol. 2, Atmospheric Propagation of Radiation*, F. G. Smith, ed., Infrared Information Analysis Center, Ann Arbor, MI and SPIE Optical Engineering Press, Bellingham WA, 1993.

[9] Tatarskii, V. I., *The Effects of the Turbulent Atmosphere on Wave Propagation*, original published in Russian in 1967, translated from Russian by Israel Program for Scientific Translations, NOAA Report TT-68-50464, U.S. Dept. of Commerce, Springfield, VA, 1971

[10] Jumper, G.Y., R.R. Beland, J.R. Roadcap, and O.R. Coté, "Effect of compressible flow on perceived temperature fluctuations measured by moving sensor", AIAA Journal, Vol. 37, No. 12, pp. 1609-1616, 1999.

[11] Vernin, J., "Atmospheric turbulence profiles", in *Wave Propagation in Random Media (Scintillation)*, University of Washington, Seattle, USA, SPIE and Inst. Of Physics publishing, Bristol and Philadelphia.

[12] Roddier, F., "The effects of atmospheric turbulence in optical astronomy", in *Progress in Optics*, E. Wolf, ed. (North-Holland, Amsterdam) Vol. **10**, 281-376, 1981.

[13] Avila, R., J. Vernin, E. Masciadri, "Whole atmosphere turbulence profiling with generalized scidar", *Appl. Opt.*, Vol. 36, pp. 7898–7905, 1997.

[14] Vernin, J and M. Azouit, "Traitement d'image adapté au speckle atmosphérique. II-analyse multidimensionnelle appliqué au diagnostic à distance de la turbulence", *J. Optics (Paris)*, **14**, 131-142 (1983).

[15] Kyrazis, D., R^3, Inc., Albuquerque, NM and F. Eaton, Air Force Research Laboratory (AFRL/DEB), KAFB, NM, personal conversation.

[1616] Otten, L. J., A. Jones, D. Black, J. Lane, R. Hugo, J. Beyer, and M. C. Roggemann, "Precision Tropopause Turbulence Measurements", *Proceedings of the SPIE on Propagation and Imaging Through the Atmosphere IV*, vol. 4125, p33 – 40, 2000.

[17] Brown, W.W., M.C. Roggemann, T.J. Schulz, T.C.Havens, J.T. Beyer, and L.J. Otten, "Measurement and data-processing approach for estimating the spatial statistics of turbulence-induced index of refraction fluctuations in the upper atmosphere", *Applied Optics*, Vol. 40, No. 12, pp. 1863-1871.